Металлофиз. новейшие технол. / Metallofiz. Noveishie Tekhnol.
2017, т. 39, № 6, сс. 779–793 / DOI: 10.15407/mfint.39.06.0779
Оттиски доступны непосредственно от издателя
Фотокопирование разрешено только
в соответствии с лицензией

МЕТАЛЛИЧЕСКИЕ ПОВЕРХНОСТИ И ПЛЁНКИ

PACS numbers: 62.20.Qp, 68.35.Ct, 68.35.Dv, 68.35.Gy, 81.15.-z, 81.40.Pq, 81.65.Lp

Mechanical and Structural Studies of Ternary Mo–Zr–N Layers Deposited on Substrate by PVD

Abdelaziz Abboudi, Brahim Chermime, Hamid Djebaili*,
and Mourad Brioua

*Department of Mechanics, Colonel Hadj Lakhdar University of Batna,
05000 Batna, Algeria*
**Department of Mechanics, Abbas Laghrour University of Khenchela,
40004 Khenchela, Algeria*

Our study of ternary Mo–Zr–N thin layers is novel with the objective of improving certain mechanical and tribological characteristics and of finding the appropriate stoichiometry to have the microstructure, which orientates to the desired properties, using the characterization techniques: SEM, XRD, EDS, XPS, WDS and similar methods as well as nanoindentation, alternative tribometry and scratch test. The morphological study of ternary Mo–Zr–N coating shows that the (111) orientation of texture is preferred essentially due to residual internal stresses. During the development of the Mo–Zr–N deposits, we have noticed that the addition of Zr results in multiphases consisting of binary ZrN, MoN and MoZrN nitrides with a prism-shaped structure. The coefficient of friction is low for Mo–N coating and low zirconium levels. The Young's modulus takes values almost very close that is indicated for values below 100 at.% of Zr. The crystalline structure does not affect the resistance capacity of the material. The introduction of zirconium particles destabilizes the compound because zirconium atomic radius (0.138 nm) is higher than that of molybdenum (0.126 nm), and the lattice is distorted that explains these residual stresses.

Keywords: microstructure, morphology, texture, hardness, Young's modulus, covers, PVD.

Corresponding author: Abdelaziz Abboudi
E-mail: abboudiabdalaziz@yahoo.fr

Please cite this article as: Abdelaziz Abboudi, Brahim Chermime, Hamid Djebaili, and Mourad Brioua, Mechanical and Structural Studies of Ternary Mo–Zr–N Layers Deposited on Substrate by PVD, *Metallofiz. Noveishie Tekhnol.*, **39**, No. 6: 779–793 (2017), DOI: 10.15407/mfint.39.06.0779.

Метою даної роботи є поліпшення механічних характеристик трикомпонентних покриттів з нітриду молібден–цирконію (Mo–Zr–N), а також пошук відповідної стехіометрії, щоб одержати мікроструктуру, орієнтовану на очікувані властивості, з використанням наступних метод характеризації: SEM, XRD, EDS, XPS, WDS та ін., а також наноіндентування, альтернативної трибометрії та випробувань за допомогою нанесення подряпин. Морфологічні дослідження трикомпонентного покриття Mo–Zr–N показали, що переважає орієнтація (111), яка, по суті, виникає завдяки залишковим внутрішнім напруженням. Під час розробки сполуки Mo–Zr–N було помічено, що додавання Zr приводить до багатофазної структури, що складається з бінарних нітридів ZrN, MoN та MoZrN з призматичною будовою. Шерсткість є меншою для покриття Mo–N та за низьких рівнів вмісту Цирконію. При цьому модулі Юнґа мають дуже близькі значення, що проявляється при концентраціях Zr, нижчих за 100 ат.%, а кристалічна структура не впливає на здатність матеріялу до опору. Введення частинок цирконію дестабілізує сполуку, оскільки атомовий радіюс Цирконію (0,138 нм) є більшим за атомовий радіюс Молібдену (0,126 нм); тому ґратниця сполуки спотворюється, що пояснює появу залишкових напружень.

Ключові слова: мікроструктура, залишкові напруження, текстура, твердість, модуль Юнга, покриття, нанесення покриття осадженням парів.

Целью данной работы является совершенствование механических характеристик трёхкомпонентных покрытий, изготовленных из нитрида молибдена–циркония (Mo–Zr–N), а также нахождение соответствующей стехиометрии, ориентированной на желаемые свойства, с использованием следующих методов характеризации: SEM, XRD, EDS, XPS, WDS и др., а также наноиндентирования, альтернативной трибометрии и испытаний с помощью нанесения царапин. Морфологические исследования трёхкомпонентного покрытия Mo–Zr–N показали, что преимущественной является ориентация (111), возникающая, по существу, благодаря остаточным внутренним напряжениям. Во время разработки соединения Mo–Zr–N было замечено, что добавление Zr приводит к многофазной структуре, состоящей из бинарных нитридов ZrN, MoN и MoZrN с призматическим строением. Шероховатость оказывается меньше у покрытия Mo–N и при низких уровнях содержания циркония. При этом модули Юнга имеют очень близкие значения, что проявляется при значениях Zr ниже 100 ат.%, а кристаллическая структура не изменяет сопротивление материала. Добавление частиц Zr дестабилизирует соединение, поскольку атомный радиус циркония (0,138 нм) больше атомного радиуса молибдена (0,126 нм); поэтому решётка соединения искажается, что объясняет образование остаточных напряжений.

Ключевые слова: микроструктура, остаточные напряжения, текстура, твёрдость, модуль Юнга, покрытие, нанесение покрытия осаждением паров.

(Received December 18, 2016; in final version, May 28, 2017)

1. INTRODUCTION

The needs for the industry in cutting devices endowed with a hardness and an excellent wear resistance, led, for several years, in the development of thin layers of nitrides of transition metals (Ti–N, Cr–N, *M*–*Y*) deposited by physical processes in vapour phase (PVD). These techniques allow putting down a superficial layer that brings remarkable improvements in the holding in service of the mechanical parts, particularly the cutting devices. These technologies are connected to the space, and we call them the nanotechnologies. The latter constitute surface treatments by application of covers with thin layers < 10 nm of thickness [1].

A considerable attention in several laboratories was just concentrated to study these covers with the vision to prepare a harder material than the diamond. Consequently, the physical limit for the maximum of the increase of the hardness in covers nanocomposite stays an open question, which is extensively studied in many laboratories [2].

The texture is strongly influenced by the conditions of deposits (conditions are preceded to elaboration, temperature, pressure of gases, bias current [3, 4]), the hardness and the tribological properties optimized are most of the time the first ones to be considered because of the potential application of these layers in the field of the manufacturing.

Parts dressed in materials with molybdenum are not enough studied during these last decades. In spite of their good mechanical properties, these covers did not find applications in the industry. Indeed, compared with the nitride of chromium, they present a coefficient of rather weak friction. They characterized by a high hardness, a weak solubility in non-ferrous alloys [5]. The formation of high-temperature oxides of Mo allows reducing the friction. Furthermore, Cr, Mo and N are important elements of addition allowing the hardening of the metallic alloys and the formation of passive films to fight against the chemical corrosion [6]. They have a good adhesion to the steel substrata because of the solubility of Mo in the ferrous alloys [7, 8] consequently.

In addition, Su *et al.* [9] had indicate that Ti–C–N is wear resistant abrasive and in the oxidation until a temperature about 800°C. Shan *et al.* [10] indeed demonstrated that the brush resistance of these films against a steel ball was better than that of the Ti–N film, because of its higher hardness and in the presence of carbon.

Nitrides of transition metals (Ti–N, Cr–N, Zr–N) were widely studied during last years. Their covers possess one high melting point, a high value of hardness and a big wear resistance, and found of numerous industrial applications.

The mechanical properties of covers Zr–N were almost close to those

of Ti–N [11, 12]. Just as there is in Ti–N, the addition of Si in the Zr–N resulted in a structure of cover nanocomposite in this study, the moderate pure hardness of the cover Zr–N (38 GPa) is extremely raised compared with the values reported usually in the literature [13]. The moderate sizes of grains exactly are not reported, but are varied between 10 nm and 20 nm according to the concentration of silicon.

Pilloud *et al.* [14] found that the addition of Si in the Zr–N makes decrease only the moderate hardness, slightly for low concentrations Si (<3.5 at.%), then largely with the addition of more Si.

As shown, if the internal stresses are too important, they control the crystalline organization of the growing deposit, and this one will turn in the direction <111> [15, 16].

The layers Zr–N won a lot of attention recently in various sectors, such as in microelectronics, as barriers of broadcasting in integrated circuits [17, 18], thanks to their weak electric resistivity [19] in comparison with Ti–N and for applications of the hard covers thanks to a big corrosion resistance [20, 21], a big hardness [22, 23], a weak coefficient of friction [24], a good adhesion with the support, and a very important electric and thermal conductivity [25, 26].

The reasons of a privileged orientation and a type of texture remained unexplained until Pelleg *et al.* [27], which have explained the crystallographic orientation of the covers PVD on the basis of a relation between the energy of surface and the residual stresses.

Nose *et al.* [28] have watch of films Zr–Si–N pulverized by RF with low concentrations Si (<13 at.%) on not warmed substrata maintained in a floating potential and have indicate that the hardest film (35 GPa) contains 3.1 at.% Si and presents a crystalline structure, and that the increase of the hardness, which varies with the content Si, can be attributed to the effect of hardening by solid solution.

Hibbs *et al.* [29] has underlined that the hardness of the layers of Ti–N decreases with the concentration of chinks at the level of the joints of grains and thus are easily deformable the hardness of the layers of Ti–N is between 2000 kg/mm^2 and 3000 kg/mm^2; however, the porosity and microcracks decrease the hardness [30]. Layers consisted of a binary Cr–N form have a low coefficient of friction and resist effectively the oxidation [31]. The speed of wear of Cr–N is compared with one for Ti–N, Zr–N, Ti–C–N, Al–Ti–N and remains lower within the tests of the 100Cr6 steel ball according to Rodriguez *et al.* [32]. The Zr–N deposits are used for the cutting of non-ferrous materials [9]. Previous studies have watch as the Cr–V–N presents a coefficient of lower friction with a low volume of wear compared to that of the Cr–N and Cr–Al–N [33]. The compounds such as Cr–W–N, Mo–Cr–N, Ti–Cr–N, Cr–Nb–N present good oxidation behaviour and a big hardness compared with the other films of Mo–N or Cr–N according to Hone *et al.* [34].

According to Su *et al.* [9], the tribological properties of Cr–N are better in comparison with the covers of Ti–N, Ti–C–N. Indeed, this type of covers presents not only a resistance increased in the wear but also a coefficient of friction enough weak that will allow to work without lubrication [1].

On the basis of this concept, textures <111>, often met in the literature, translate the presence of strong residual stresses within the deposits [35, 36].

The research works, which we began at the level of the LaboMap ENSAM (LaboMap Mechanical and Industrial Engineering School) of Cluny, first of all, were preceded by a bibliographical study summarizing the results of the researchers in the field of the nanotechnology and more exactly that of the thin layers (binary and ternary). The current work begins with a summary of data and the objectives follow-up of an introduction. Therefore, we have showed the material and the equipment, which we have used to make our experimental tests followed by the results and the discussions. The study is divided to a structural one characterized by the AFM, XRD and mechanical tests analysed hardness, roughness and tribological properties. We draw, at the end of work, the adequate consequences expressed in the form of conclusion, which regroups the results by comparing it with the objectives, which leave the open door towards profound investigations of new materials likely to be submitted to strong thermal, mechanical or chemical requests forced in search of new effective solutions.

2. EXPERIMENTAL DEVICES AND MATERIAL USED

Figure 1 shows machine that practices vacuum deposits.

The quality of the measurements is sufficient for the identification of the phases, the texture (preferential orientation of the grains) and the determination of the lattice parameter.

The half-height width of the diffraction peak can be used to deduce the defects, which are at the origin of the non-uniform stress distribution often observed in PVD deposits.

The recording of force between the ends of the beam makes it possible to produce images (Fig. 2) in order to measure the roughness of the surface studied up to a resolution close to the atomic scale (in contact mode) as well as to determine the grain size or qualify the porosity of a layer. The three dimensions can be controlled by the tip; we can directly obtain an image of the surface, with a depth resolution of 0.01 nm and a lateral resolution of 0.1 nm [37].

Figure 3 shows hardness-testing machine.

The impressions were carried out using a hardness-testing machine, Testwell–Testor HT la, equipped with a Brinell indenter. A 2.5 mm diameter ball was used. For each sample of coated XC100, two tests were

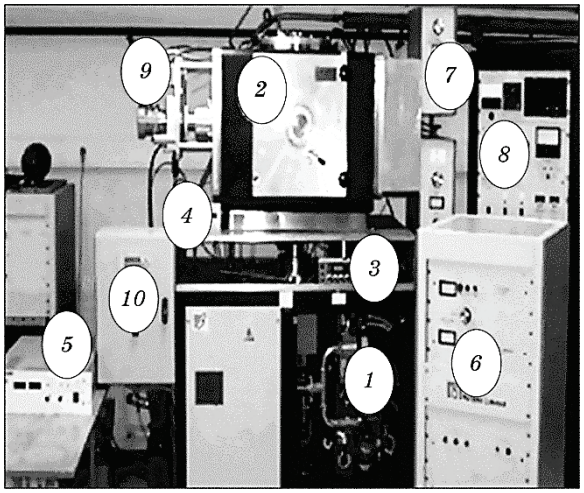

Fig. 1. Magnetron sputtering system: *1*—pumping system, *2*—filing cabinet, *3*—mass flowmeters, *4*—pressure drive, *5*—DC power supply, *6*—13.56 MHz RF generator, *7*—stub, *8*—quadrant control, *9*—turntable motor substrate holder (PS), *10*—automaton.

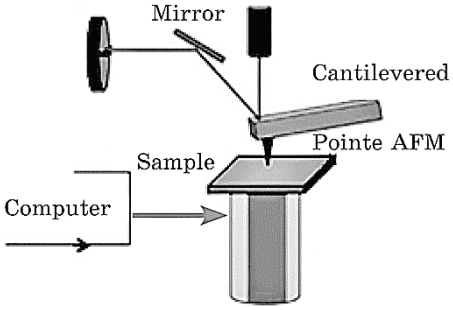

Fig. 2. Illustration of the Principe of the Atomic Force Microscope.

performed using standard parameters (1860 N).

Table 1 shows composition of the XC100 steel.

3. PREPARATION OF SAMPLES

Preparation of Substrates

Si. From clean square or non-square substrates in one wafer of one-side polished Si(100) (cut on the polished side) using the diamond stylus and a ruler, we make samples of 1 cm×1 cm. The Si thickness is 380 μm.

XC100 Steel. We check the R_a (average) and R_t (peak-to-peak) parame-

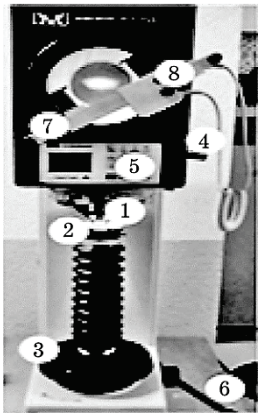

Fig. 3. Hardness Testing Machine (Testwell–Testor HT laBoMaP): *1*—support pin for Rockwell B (diameter bead) and optical microscope, *2*—clamp, *3*—approach vice with mam, *4*—the type selector, *5*—monitor and program selector 15.6–250 kg, *6*—manoeuvring level, *7*—rule for the dimensions, *8*—validation button measurement.

TABLE 1. Chemical composition of XC100 steel, wt.%.

XC100	C	Mn	SP	Si	Cr	Ni	Cu
% wt.	0.95	0.25	S < 0.025	0.15	0.15	0.20	0.20

ters of roughness of the current samples having R_a of the order of 200 nm to 500 nm maximum and R_t of 1 μm maximum. These parameters have low values, but same ones for all samples.

We determine the number of square Si for constraints, other (non-square) for composition, XRD, MEB, *etc.* (But not too small both to put at each deposit and to obtain enough for all the characterizations to be done thereafter.)

Similarly, we calculate the n_b of steel samples to be put for each deposit, thus, the total n_b of samples to be prepared, so that it is necessary to optimize the placement of the samples on the substrate holder (steels and Si), and to always put them in the same place at each deposit for reproducibility. (NB: consider keeping a sample of each (Si and steel) for future analyses (1 Si and 1 steel).)

Cleaning of Substrates

Before loading a substrate (Si or steel) into the enclosure, it must be cleaned *ex situ* as following: put alcohol at 95° in the ultrasonic bottom and then put samples in a beaker with both trichloroethylene (99.5%)

for 5 min, pure acetone (99.5%) for 5 min, and ethanol (99.5%) for 5 min. At the end of each stage, the substrates are rinsed with deionizer water and stored in pill bottles containing absolute ethanol (for Si) or in a desiccators for steels (to avoid oxidation) up to their usage. (NB: clean the Si assemblies (all of them clean all at once) and the steels in several steps do not put steels with Si at the risk of damaging them.)

Check that you have cleaned the chamber and that you have the correct target (especially that of Mo) mounted on a cathode and mark it (top or bottom to know the RF generator and the tuning box to use). To check the cleanliness of the enclosure, iron an absorbent paper cleaning substrates *in situ* and target to be done before each deposit when residual vacuum reaches around 10^{-6} mbar or $8{\cdot}10^{-7}$ mbar on Alcatel gauge procedure but apply 12 kV with the HT generator for 5 min on substrates and target under Ar. (NB: for the first deposit, after the machine has been stopped for more than 3 months, strike the target at least 15 min under Ar.)

Pre-Pulverizing the Target

The pre-pulverizing operation consists in placing the target under the deposition conditions for a time of 5 min to 10 min. The target, after ionic cleaning, is not nitride. Therefore, there is a transient state under unstable conditions. Since some of the deposits have durations of the order of 5 min to 10 min, this transient state introduces an error, which can be not negligible in the calculation of the deposition rates. It is therefore necessary to nitride the target before starting the deposition.

4. CHARACTERIZATION, RESULTS, DISCUSSION AND ANALYTICAL METHODS

4.1. The Atomic Force Microscopy

The atomic force microscopy (AFM) is a widely used technique for providing images of sample surface. It reaches very high-resolution levels up to the atomic level. Therefore, we can make images of surfaces with a very high resolution. When the tip approaches the surface of the sample (at a distance of a few tenths of nanometre), forces of van der Waals interaction between the atoms of the tip and those of the test surface cause cantilever bending and deflection of the controlling beam depended on the distance between surface and sample. The main mode of use of an AFM is based on the use of a feedback loop to maintain a constant distance between the tip and the analysed surface by means of a piezoelectric actuator. Images (3 μm×3 μm) of the surface of

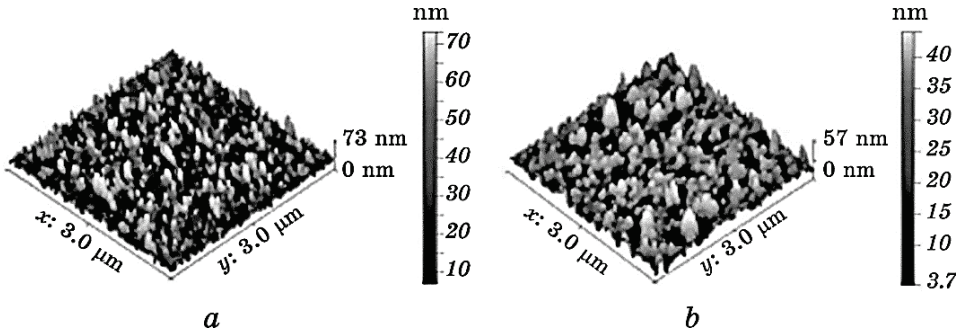

Fig. 4. The structure of Mo–N (*a*) and Mo–Zr–N (*b*). It appears that the particle size of about 80 nm randomly dispersed.

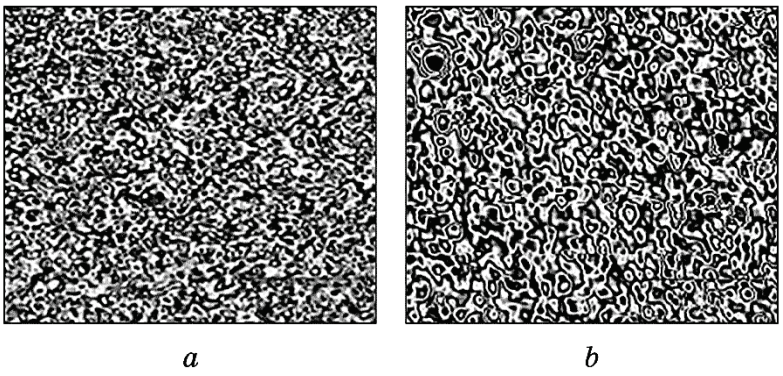

Fig. 5. Surface morphologies of Mo–N (*a*) and Mo–Zr–N (*b*).

some of our films were obtained using a constant force of 0.035 N/m and determined their respective roughness. It is observed in the AFM images Fig. 4; the surface density of the columns decreases with the thickness, so the columns are bigger.

The layers must show a hardness decreases as their thickness increases. Note that the roughness decreases with the width of the column. The roughness varies from 44 nm to 3.7 nm for the Mo–Zr–N coating and from 73.2 nm to 2 nm for the Mo–N coating.

Indeed, at the beginning of the growth of the layer, it is first creating islands that will coalesce and hinder the movement of dislocations (see Fig. 5).

4.2. XRD Data

The x-ray diffraction spectra were recorded using X'PERT PRO MRD type diffractometer from Panalytical, equipped with a copper anode

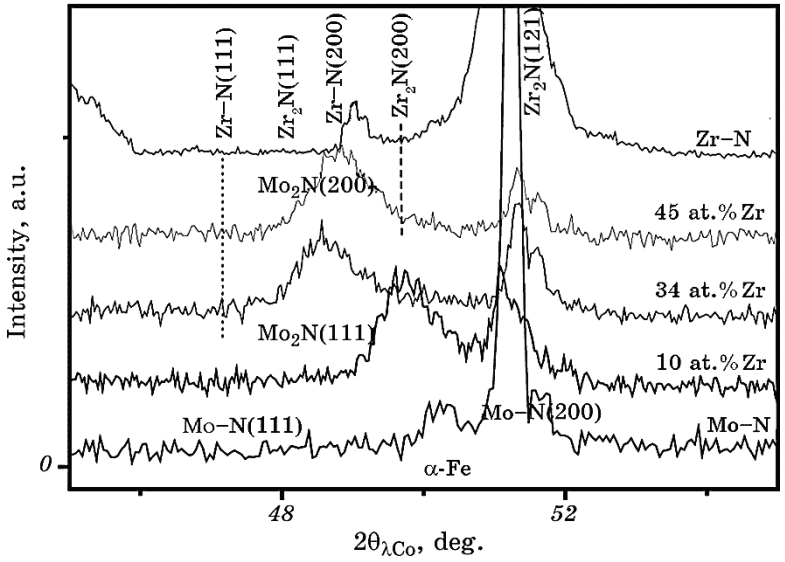

Fig. 6. XRD patterns of Mo–N, Mo–Zr(10 at.% Zr)–N, Mo–Zr(34 at.% Zr)–N, Mo–Zr(45 at.% Zr)–N, Zr–N.

XR-tube. An acquisition time of 5 s per angular step of 0.04° was used over the interval between 30° and 55° (2θ).

The identification of the crystalline phases presented was made by comparing the observed lines with those of the appropriate phases contained in the PDF-2 database.

Deposits of Zirconium Nitride. XRD spectra of deposits of the zirconium nitride with different concentrations of Zr on the XC100 steel are presented in Fig. 6. The observed peaks reveal the presence of ZrN, Zr_2N, MoN, Mo_2N, and MoZrN phases of cubic structure (JCPDS not 004–0850).

Peaks of the phases ZrN, Zr_2N with orientation (111) and (200) between the angles 2θ equal 40° and 50° are explained by the strong presence of residual stresses.

4.3. Parameter of Deposition and Crystallite Size

Below, there is a summary of data with the corresponding results (Table 2). The potential of Mo and Zr is varied with the power of the plasma in stoichiometric proportions of Ar/N_2; N/(Zr + Mo) is obtained and the thickness (*e*) increases when Zr is added.

When there is no more Mo, then the thickness decreases considerably (see corresponding mesh parameters in Table 2).

The ternary Mo–Zr–N is taken, and the zirconium level is gradually varied (0 at.%, 10 at.%, 34 at.%, 45 at.%, 100 at.%). The results are

TABLE 2. Parameter of deposition (P, U), crystallite size of Mo–N, Mo–Zr–N and Zr–N coatings, thickness (e), and elements concentrations (in atomic percent).

Deposit		Mo–N	$Mo_{0.39}Zr_{0.1}N_{0.48}$	$Mo_{0.14}Zr_{0.34}N_{0.48}$	$Mo_{0.06}Zr_{0.45}N_{0.48}$	Zr–N
Gas	Ar/N_2	75/25				
Mo	P_{Mo}, W	640	640	650	350	–
	U_{Mo}, V	900	850	850	500	–
Zr	P_{Zr}, W	–	300	650	650	650
	U_{Zr}, V	–	550	900	800	–900
N		48.9	48.4	48.5	47.5	47.4
Mo		49.0	39.6	14	5.5	–
O		2.1	2.0	3.5	2.0	4.6
Zr		–	10	34	45	48.8
N/(Mo + Zr)		0.997	0.97	1.01	0.94	0.97
e, μm		1.36	1.42	1.64	2.2	1.3

recorded increasing a peak (34 at.%, 25 GPa) for Mo–N (18.5 GPa) and Zr–N (15 GPa) in Fig. 7.

The Young's modulus takes values almost close that explains, for the values below 100 at.% of Zr, the same resistance (Fig. 8).

The residual stress is compressive and is computed with the Stoney formula [38]:

$$\sigma = \pm \frac{E_s}{6(1-\nu_s)} \frac{e_s^2}{e_f} \left(\frac{1}{R} - \frac{1}{R_0} \right),$$

where σ is the residual stress in the thin film, E_s and ν_s are Young's modulus (195 GPa) and Poisson's ratio (0.29) of the substrate, e_f and e_s indicate the film and substrate thicknesses, respectively, R is the curvature radius of the sample after deposition, R_0 is the curvature radius before deposition.

The decrease of the stress, when the thickness increases, is attributed to relaxation of the layer in surface. It is noted that the stress of Zr–N layers (Fig. 9) is not constant with the thickness. It reaches a maximum and then decreases to 100 nm to 250 nm. Such results have been reported for layers of aluminium nitride [39]. The stress peak is due to a change in structure during growth of the layer.

The most important residual stress is at 34 at.% Zr with a value of 1.9 GPa. Therefore, Mo–N and Zr–N are less strained than Mo–Zr–N;

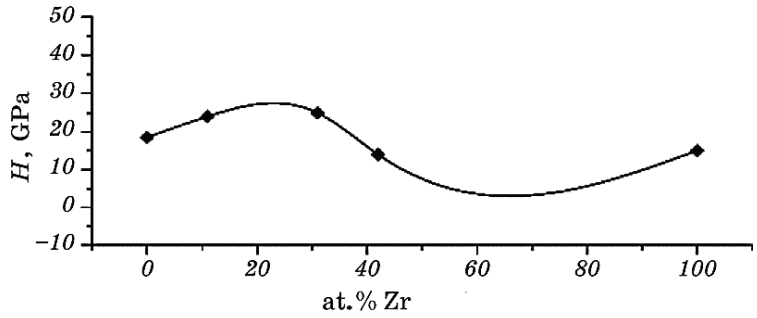

Fig. 7. Hardness of Mo–Zr–N layer as a function of at.% Zr.

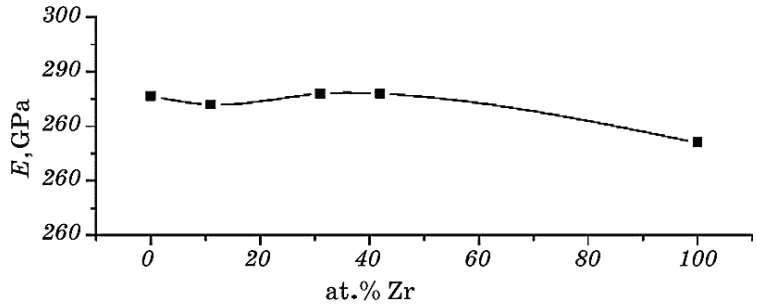

Fig. 8. Mo–Zr–N layer Young's module as a function of at.% Zr.

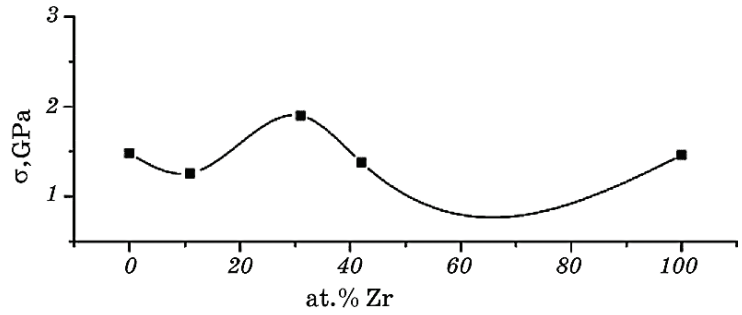

Fig. 9. Residual stresses of Mo–Zr–N layer as a function of at.% Zr.

the introduction of zirconium particles destabilizes the compound that is essentially due to the intrinsic and thermal stresses.

5. CONCLUSION

The results of researchers in the field of deposits of the ternary and binary nanolayers note that the compounds most used for their hardness

such as Cr–N, Ti–C–N, Cr–W–N, Al–Ti–N, Zr–Si–N, Ti–C–N resistant to abrasive wear and oxidation to a temperature of about 800°C and that the resistance to friction is better than that of Ti–N.

Cr–N films tend to replace Ti–N films because they have very good corrosion resistance, good stability at high temperature, and thick layers are required. The study on deposits about our work that remain unexplored was approached by a bibliographic search, which highlights the current state of research and the experimental chapter on compounds: Mo–N, Zr–N, Mo–Zr–N.

The morphological study of the ternary Mo–Zr–N deposit showed that an orientation given by the dexterities of the textures (111) and (222) is due to residual internal stresses.

The Mo–N coating is less hard than the Cr–N one, however, catchier and adheres more into the substrate; Zr–N deposit is hard, but does not have great grip. Now for the addition of zirconium in the molybdenum nitride, the hardness passes through a maximum at 31 at.% Zr, and residual stresses maximum is at 42 at.% Zr. The coefficient of friction is low for Mo–N and Zr–N with respect to Mo–Zr–N; the roughness is good for Mo–Zr–N deposits with low zirconium concentrations.

The Mo–Zr–N coating has a maximum hardness with zirconium concentration and is less corrosion resistant than Cr–N.

With regard to hardness, we gradually vary the zirconium content by 0 at.%, 10 at.%, 34 at.%, 45 at.% up to 100 at.%; the results for the hardness fluctuate up to a maximum (25 GPa) observed at 31 at.% Zr; for Mo–N and Zr–N hardness takes values of 18.5 and 15 GPa, respectively. The potential is also varied between 550, 900, 800, –900 V, and the corresponding power values are as follow: 300, 650, 650, 650 W.

The Young's modulus takes values almost very close, which is indicated for values below 100 at.% of Zr; so, the crystal structure does not influence the resistance capacity.

Conversely, the most important residual stress is at 31 at.% Zr with a value of 1.9 GPa. Therefore, Mo–N and Zr–N coatings are less strained than Mo–Zr–N coating; the introduction of the zirconium particles destabilizes the compound, which is an essentially intrinsic and thermal deposit.

REFERENCES

1. Brahim Tlili, *Caractérisation de Films durs Multicouches Élaborés par Pulvérisation Magnétron. Influnce des Conditions d'Élaboration sur Leurs Propriétés* (Thèse de Doctorat) (Arts et Métiers Paris-Tech: Institut des Sciences et Technologies: 2010) (in French).
2. Kezai, *Characterization of Interfacial Reactions in Binary and Multiple Metallic Thin Films* (Thèse de Doctorat) (Arts et Métiers Paris-Tech: Institut

des Sciences et Technologies: 2007) (in French).
3. A. S. Korhonen, *Vacuum*, **45**, Iss. 10–11: 1031 (1994).
4. M. I. Jones, I. R. McColl, and D. M. Grant, *Surf. Coat. Technol.*, **132**, Iss. 2–3: 143 (2000).
5. J.-C. Chuang, S.-L. Tu, and M.-C. Chen, *Thin Solid Films*, **346**, Iss. 2–3: 299 (1999).
6. J.-B. Lee, *Mater. Chem. Phys.*, **99**, Iss. 2–3: 224 (2006).
7. C. Scandian, C. Boher, J. D. B. de Mello, and F. Rézai-Aria, *Wear*, **267**, Iss. 1–4: 401 (2009).
8. K. Frisk, *Calphad*, **15**, Iss. 1: 79 (1991).
9. Y. L. Su, S. H. Yao, Z. L. Leu, C. S. Wei, and C. T. Wu, *Wear*, **213**, Iss. 1–2: 165 (1997).
10. L. Shan, Y. Wang, J. Li, H. Li, X. Wu, and J. Chen, *Surf. Coat. Technol.*, **226**: 40 (2013).
11. W. D. Sproul, *Thin Solid Films*, **107**, Iss. 2: 141 (1983).
12. P. C. Johnson and H. Randhawa, *Surf. Coat. Technol.*, **33**: 53 (1987).
13. J.-H. Huang, C.-Y. Hsu, S.-S. Chen, and G.-P. Yu, *Mater. Chem. Phys.*, **77**, Iss. 1: 14 (2003).
14. D. Pilloud, J. F. Pierson, A. P. Marques, and A. Cavaleiro, *Surf. Coat. Technol.*, **180–181**: 352 (2004).
15. L. Krusin-Elbaum, M. Wittmer, C. Y. Ting, and J.-J. Cuomo, *Thin Solid Films*, **104**, Iss. 1–2: 81 (1983).
16. M.-B. Takeyama, T. Itoi, E. Aoyagi, and A. Noya, *Appl. Surf. Sci.*, **190**, Iss. 1–4: 450 (2002).
17 S. Horita, M. Kobayashi, H. Akahori, and T. Hata, *Surf. Coat. Technol.*, **66**, Iss. 1–3: 318 (1994).
18. U. K. Wiiala, I. M. Penttinen, and A. S. Korhonen, *Surf. Coat. Technol.*, **41**, Iss. 2: 191 (1990).
19. L. van Leaven, M. N. Alias, and R. Brown, *Surf. Coat. Technol.*, **53**, Iss. 1: 25 (1992).
20. P. Panjan, B. Navinšek, A. Žabkar, V. Marinković, Dj. Mandrino, and J. Fišer, *Thin Solid Films*, **228**, Iss. 1–2: 233 (1993).
21. E. Kelesoglu, C. Mitterer, M. K. Kazmanli, and M. Ürgen, *Surf. Coat. Technol.*, **116–119**: 133 (1999).
22. R. J. Rodríguez, J. A. García, A. Medrano, M. Rico, R. Sánchez, R. Martínez, C. Labrugère, M. Lahaye, and A. Guette, *Vacuum*, **67**, Iss. 3–4: 559 (2002).
23. S. Horita, M. Kobayashi, H. Akahori, and T. Hata, *Surf. Coat. Technol.*, **66**, Iss. 1–3: 318 (1994).
24. J. Pelleg, L. Z. Zevin, and S. Lungo, N. Croitoru, *Thin Solid Films*, **197**, Iss. 1–2: 117 (1991).
25. M. Nose, W. A. Chiou, M. Zhou, T. Mae, and M. Meshii, *J. Vac. Sci. Technol. A*, **20**: 823 (2002).
26. M. K. Hibbs, B. O. Johansson, J.-E. Sundgren, and U. Helmersson, *Thin Solid Films*, **122**, Iss. 2: 115 (1984).
27. S. Labdi, Ph. Houdy, P. Psyllaki, and M. Jeandin, *Thin Solid Films*, **275**, Iss. 1–2: 213 (1996).
28. A. Pan and J. E. Greene, *Thin Solid Films*, **78**, Iss. 1: 25 (1981).
29. R. J. Rodríguez, J. A. García, A. Medrano, M. Rico, R. Sánchez,

R. Martínez, C. Labrugère, M. Lahaye, and A. Guette, *Vacuum*, **67**, Iss. 3–4: 559 (2002).
30. V. G. Ivanchenko and T. V. Mel'nichenko, *Metallofizika*, **13**, No. 2: 23 (1991).
31. M. Uchida, N. Nihira, A. Mitsuo, K. Toyoda , K. Kubota, and T. Aizawa, *Surf. Coat. Technol.*, **177–178**: 627 (2004).
32. Y. Benlatreche, *Contribution à L'amélioration de la Durée de vie D'outils Carbure pour L'usinage du MDF (Medium Density Fiberboard) par Application de Dépôts Ternaires (CrAlN, CrVN) et Modification de L'arête de Coupe* (Thèse de Doctorat) (Arts et Métiers Paris-Tech: Institut des Sciences et Technologies: 2011) (in French).
33. J. Musil, *Surf. Coat. Technol.*, **125**, Iss. 1–3: 322 (2000).
34. M. Odén, J. Almer, G. Håkansson, and M. Olsson, *Thin Solid Films*, **377–378**: 407 (2000).
35. R. Novák, I. Kvasnička, D. Nováková, and Z. Malá, *Surf. Coat. Technol.*, **114**, Iss. 1: 65 (1999).
36. A. Lousa, J. Romero, E. Martínez, J. Esteve, F. Montalà, and L. Carreras, *Surf. Coat. Technol.*, **146–147**: 268 (2001).
37. W. Grzesik, *Advanced Machining Processes of Metallic Materials* (Elsevier Science: 2008).
38. G. G. Stoney, *Proc. R. Soc. A*, **82**, Iss. 553: 172 (1909).
39. Y. L. Di, Z. H. Cai, P. Zhang, and W. Shen, *Adv. Mater. Res.*, **557–559**: 1650 (2012).